6646 *Biochemistry* **2010,** *49,* 6646–6654
DOI: 10.1021/bi100692f

BIOCHEMISTRY
including biophysical chemistry & molecular biology
Article

Kinetic and Spectroscopic Studies of Hemin Acquisition in the Hemophore HasAp from *Pseudomonas aeruginosa*[†]

Erik T. Yukl,[‡,||] Grace Jepkorir,[§] Aileen Y. Alontaga,[§] Lawrence Pautsch,[‡] Juan C. Rodriguez,[§] Mario Rivera,[§] and Pierre Moënne-Loccoz*[,‡]

[‡]*Department of Science and Engineering, School of Medicine, Oregon Health and Science University, 20000 Northwest Walker Road, Beaverton, Oregon 97006-8921, and* [§]*Department of Chemistry, University of Kansas, Lawrence, Kansas 66047.* [||]*Current address: Department of Biochemistry, Molecular Biology and Biophysics, University of Minnesota, Minneapolis, MN 55455.*

Received May 4, 2010; Revised Manuscript Received June 28, 2010

ABSTRACT: The extreme limitation of free iron has driven various pathogens to acquire iron from the host in the form of heme. Specifically, several Gram-negative pathogens secrete a heme binding protein known as HasA to scavenge heme from the extracellular environment and to transfer it to the receptor protein HasR for import into the bacterial cell. Structures of heme-bound and apo-HasA homologues show that the heme iron(III) ligands, His32 and Tyr75, reside on loops extending from the core of the protein and that a significant conformational change must occur at the His32 loop upon heme binding. Here, we investigate the kinetics of heme acquisition by HasA from *Pseudomonas aeruginosa* (HasAp). The rate of heme acquisition from human met-hemoglobin (met-Hb) closely matches that of heme dissociation which suggests a passive mode of heme uptake from this source. The binding of free hemin is characterized by an initial rapid phase forming an intermediate before further conversion to the final complex. Analysis of this same reaction using an H32A variant lacking the His heme ligand shows only the rapid phase to form a heme−protein complex spectroscopically equivalent to that of the wild-type intermediate. Further characterization of these reactions using electron paramagnetic resonance and resonance Raman spectroscopy of rapid freeze quench samples provides support for a model in which heme is initially bound by the Tyr75 to form a high-spin heme−protein complex before slower coordination of the His32 ligand upon closing of the His loop over the heme. The slow rate of this loop closure implies that the induced-fit mechanism of heme uptake in HasAp is not based on a rapid sampling of the H32 loop between open and closed configurations but, rather, that the H32 loop motions are triggered by the formation of the high-spin heme−HasAp intermediate complex.

Certain opportunistic pathogens, such as *Pseudomonas aeruginosa*, are able to overcome the extremely low levels of available free iron within their mammalian host by deploying several iron acquisition systems. One of these, encoded by the *has* (heme acquisition system) operon found in a number of Gram-negative bacteria, involves the secretion of a heme-binding protein HasA[1] (*1*). HasA binds extracellular heme with high affinity (5.3×10^{10} M^{-1}) (*2*) and delivers it to a specific outer membrane receptor, HasR (*1*, *3*). Once the heme is imported into the cell, heme oxygenases degrade it, providing the organism with a source of iron (*4*). This is an effective strategy given that heme, as opposed to "free" iron, is abundant within the mammalian host, with hemoglobin (Hb) representing a particularly large reservoir. *P. aeruginosa* maximizes the utilization of this reservoir by secreting hemolysins (*5*, *6*) and cytotoxins (*7*) to lyse the host's erythrocytes, liberating Hb.

HasA from *P. aeruginosa* (HasAp) has been shown to be essential for the growth of this organism using Hb as the sole iron source (*8*), thus supporting its vital role in the acquisition of heme from Hb. However, the mechanism by which this process occurs is still under debate. The inability of ultracentrifugation experiments to detect a stable complex between human met-Hb and apo-HasA from *Serratia marcescens* (HasAs) suggests a passive mode of acquisition, with HasAs binding heme only subsequent to its dissociation from met-Hb (*9*, *10*). Such a mechanism may be sufficient given that rapid dilution of oxy-Hb upon erythrocyte lysis promotes dissociation of Hb into $\alpha\beta$ dimers (*11*, *12*), acceleration of autoxidation (*13*), and hemin dissociation (*14*). Conversely, NMR analyses of mixtures of holo-HasAp and human met-Hb show perturbations consistent with the formation of a transient complex between these two proteins (*15*). Knowing that the rates of dissociation of heme from met-Hb, at various concentrations, have been carefully studied (*14*), we set out to measure the rate of heme acquisition from met-Hb by apo-HasAp to determine whether the formation of a transient complex facilitates the loss of heme from met-Hb. To the best of our knowledge, such experiments have not been reported for HasAp and its homologues.

[†]This work was supported in part by the National Science Foundation (P.M.-L., MCB-0811888; M.R., MCB-0818488) and the National Institutes of Health (P.M.-L., GM 74785; M.R., GM 50503).

*To whom correspondence should be addressed: Oregon Health and Science University, 20000 NW Walker Rd., Beaverton, OR 97006. Telephone: (503) 748-1673. Fax: (503) 748-1464. E-mail: ploccoz@ebs.ogi.edu.

[1]Abbreviations: HasA, heme binding protein acquisition; HasR, HasA-specific outer membrane receptor; met-Hb, met-hemoglobin; RFQ, rapid freeze quench; RR, resonance Raman; EPR, electron paramagnetic resonance; HEPES, *N*-(2-hydroxyethyl)piperazine-*N*'-2-ethanesulfonic acid; HS/LS, high-spin/low-spin.

 Published on Web 06/29/2010

Also of interest is the possibility of observing intermediates in the process of binding heme to apo-HasAp. Structural characterizations of HasAp (*15*, *16*) and HasAs (*17*−*19*) show that these ~19 kDa proteins adopt a monomeric structure composed of an extended antiparallel β-sheet and a four-α-helix wall from which extrudes two loops that sandwich the heme molecule. The Fe(III) heme is axially coordinated by His32 and Tyr75 which also engages in a hydrogen bond interaction with His83 (*15*, *17*). In the apo form of the hemophore, the loop bearing Tyr75, the latter of which is largely unaffected by the absence of the heme molecule and the interaction between Tyr75 and His83 is maintained, but the His32 loop adopts a very different conformation (*16*, *19*). Specifically, the His32 loop moves 30 Å away from the heme binding site to interact with the outer surface of the protein core. This open configuration of the apo form led Wolff and co-workers to propose an "induced-fit" model of the heme uptake process in HasA, with a two-step mechanism where the heme interacts first with the Tyr75 loop before the heme pocket closes. Closure of the His32 loop over the heme is presumably mediated by the binding of His32 to the heme iron and by the formation of hydrogen bonds between heme propionate groups and backbone nitrogen atoms of the His32 loop (*18*, *19*). Several other indirect lines of evidence support the idea that Tyr75 is the predominant of the two axial ligands: (1) Among HasA homologues from four Gram-negative bacteria, His32 is conserved among only three while the Tyr75/His83 pair is fully conserved (*20*); (2) While mutation of either Tyr75 or His83 to Ala results in a loss of binding affinity of 2 orders of magnitude in HasAs, the affinity of H32A HasAs is decreased by only 5-fold relative to that of the wild type (wt) (*2*); (3) Formation of a Fe(II)−CO complex in both wt and H83A HasAs proceeds by displacement of His32 rather than Tyr75 (*21*); (4) Crystal structures of holo-HasAs in complexes with wt and variant HasR receptor proteins show the heme iron(III)−Tyr75 coordination retained while the H32 loop is disordered (*22*). The fact remains that direct evidence of a two-step mechanism for the heme uptake process in HasA is lacking.

In this work, we strive to answer two fundamental questions about heme binding by HasAp: (1) Does the transient complex that has been proposed to form between HasAp and human Hb (*15*) enhance the rate of heme loss from Hb; and (2) What is the mechanism by which apo-HasAp binds hemin? Specifically, can we identify intermediate(s) coordination in the hemin binding process and determine which ligand initially binds the iron or whether both ligands bind simultaneously. Intermediates are not observed in the hemin binding reactions of the six-coordinate hemophores HtsA [likely His/Met ligation (*23*, *24*)] or Shp [bis-Met ligation (*25*)], but the asymmetric His/Tyr ligation and the structural differences in the ligand-carrying loops in HasAp could lead to distinct hemin binding kinetics. To answer the first question, we followed the transfer of heme from human met-Hb to apo-HasAp using UV−vis spectroscopy and compared the rate of transfer to literature values for the rate of dissociation of heme from met-Hb. To address the hemin binding mechanism, we analyzed the kinetics of hemin binding to wt and H32A apo-HasAp using stopped-flow spectroscopy. We also characterized rapid freeze quench (RFQ) samples of these reactions using resonance Raman (RR) and EPR spectroscopy. The work presented here demonstrates that wt apo-HasAp acquires free hemin in two steps via the formation of a coordination intermediate equivalent to the resting state of H32A holo-HasAp before completion of the heme binding pocket with a $t_{1/2}$ in the hundred millisecond range ($k \sim 5\ s^{-1}$ at 4 °C).

MATERIALS AND METHODS

Expression and Purification of apo-HasAp. The truncated form of HasAp, omitting the last 21 C-terminal amino acids, was constructed as described previously (*15*). The H32A mutation was introduced by site-directed mutagenesis using the QuickChange mutagenesis kit (Stratagene), and the mutation was confirmed by DNA sequencing (SeqWright). The plasmid was transformed into *Escherichia coli* BL21 GOLD (DE3) competent cells for subsequent protein expression. A 50 mL starter culture in Luria-Bertani (LB) medium (100 μg/mL ampicillin) was grown overnight in a 125 mL flask from a single colony of transformed cells from a freshly streaked LB agar ampicillin plate. The growth was used to inoculate 30 mL of M9 minimal medium containing 200 μg/mL ampicillin and grown to an OD_{600} of 0.8−0.9. The cells were centrifuged at 4800 rpm for 10 min at 4 °C, resuspended in 1.0 L of fresh minimal M9 medium (200 μg/mL ampicillin), and cultured to an OD_{600} of ~0.9 at 37 °C. The temperature was decreased to 30 °C with continuous incubation to an OD_{600} of ~1.0, and protein expression was induced with the addition of isopropyl β-D-thiogalactopyranoside (IPTG) to a final concentration of 1 mM. After being cultured for 5 h, the cells were harvested and stored at −20 °C. The pellet was resuspended in 20 mM Tris-HCl (pH 7.6) (3 mL/gram of cell paste), and DNase (Sigma-Aldrich, St. Louis, MO) was added; the cells were disrupted by sonication, and the cell debris was separated by centrifugation at 19500 rpm and 4 °C for 40 min. Purification of wild-type apo-HasAp or its H32A mutant was conducted by ion exchange chromatography at 4 °C and by hydrophobic interaction chromatography at ambient temperature. The clarified supernatant obtained after removal of cell debris was loaded onto a Q-Sepharose Fast Flow column [2.6 cm inside diameter × 15 cm (GE Healthcare)] pre-equilibrated with 20 mM Tris-HCl (pH 7.6). The column was washed with at least 3 bed volumes of the same buffer before protein elution with a linear NaCl concentration gradient (from 0 to 600 mM). Fractions containing HasAp were pooled and exchanged into 50 mM sodium phosphate buffer containing 0.7 M ammonium sulfate (pH 7.0) prior to being loaded onto a Butyl Sepharose Fast Flow (GE Healthcare) column (2.6 cm inside diameter × 12 cm) equilibrated with the same buffer. Elution of weakly bound contaminating proteins and holo-HasAp was achieved with 50 mM sodium phosphate and 0.5 M ammonium sulfate, before elution of apo-HasAp with a linear gradient of sodium phosphate buffer (from 50 to 20 mM) and ammonium sulfate (from 0.50 to 0 M). Fractions containing the apoprotein were loaded onto a Phenyl Sepharose 6 Fast Flow high substitution (GE Healthcare) column (2.6 cm inside diameter × 12 cm) and eluted using the two steps described above. The purity of the protein in the resultant fractions was assessed by SDS−PAGE, and if necessary, fractions containing apo-HasAp were purified again on a second Butyl Sepharose column. The MW of wild-type and H32A apo-HasAp was determined by electrospray mass spectrometry.

Transfer of Heme from Hemoproteins to wt apo-HasAp. Electronic absorption spectra were recorded using a Cary 50 Varian spectrophotometer using a resolution of 1 nm and a scanning rate of 1200 nm/min. The concentration of wt apo-HasAp was determined by titration with a solution of bovine hemin (Sigma). Lyophilized human Hb (Sigma) was dissolved in phosphate buffer ($\mu = 0.1$, pH 7.0) and purified in a Sephacryl S-200 size exclusion column pre-equilibrated and eluted with phosphate buffer ($\mu = 0.1$, pH 7.0). Fractions with a purity ratio

(A_{280}/A_{406}) of <0.25 were pooled and concentrated using Amicon ultracentrifuge filters to a final concentration of 3.5 mM. This purification process was necessary to remove adventitiously bound hemin which would confound the results of the experiment. Purified Hb was then incubated with a 10-fold excess of potassium ferricyanide (Mallinckrodt) for 10 min followed by removal of excess ferricyanide using desalting spin columns [Zeba, 0.5 mL (Pierce)]. Reactions were initiated by mixing Hb and wt apo-HasAp solutions to final concentrations of 50 μM (in heme) and 200 μM, respectively, in 50 mM HEPES (pH 7.0) containing 150 mM NaCl. Solutions were loaded into 2 mm path length cuvettes, and scans were taken every 5 min for 120 min. For transfer reactions from reduced Hb, concentrated solutions of met-Hb and wt apo-HasAp were purged of oxygen with Ar and brought into a glovebox with a controlled atmosphere of <1 ppm O_2 (Omni-Lab System, Vacuum Atmospheres Co.). Met-Hb was diluted in the buffer described above, and sodium dithionite was added to a final concentration of 500 μM. Reduced Hb was loaded into a 2 mm path length cuvette and the cuvette was sealed. Reactions were initiated by the injection of anaerobic wt apo-HasAp to final concentrations of 200 and 50 μM in Hb heme. Horse heart Mb (Sigma) was oxidized with ferricyanide as described above and desalted twice to remove excess ferricyanide and adventitiously bound heme. Heme transfer reactions were conducted in a manner identical to that of the reactions for met-Hb. Single-wavelength absorbance data were fit to a double-exponential expression with identical amplitudes using Origin 7.0 (Origin Lab Corp.).

Stopped-Flow UV−Vis Spectroscopy. The concentrations of stock wt and H32A apo-HasAp solutions were determined as described above to yield extinction coefficients at 280 nm of 28.6 and 29.8 mM^{-1} cm^{-1}, respectively. These values were subsequently used to determine apo-HasAp concentrations in reaction mixtures. Hemin was dissolved in 10 mM NaOH, and its concentration was determined using an ε_{385} of 58.4 mM^{-1} cm^{-1} (*26*); this was diluted to a final concentration of 13 μM in 10 mM NaOH and used immediately. Apoproteins were diluted in 200 mM HEPES (pH 7.5). Solutions were loaded into an SX20 stopped-flow UV−vis spectrometer (Applied Photophysics) equilibrated to 4.2 °C. Excess solution was recovered from the stopped-flow apparatus after each experiment to remeasure the concentrations of hemin and apo-HasAp after loading; this was necessary due to the design of the instrument, which leads to some sample dilution upon loading. Controls using 1:1 mixtures of hemin solution and buffer were run to ensure that the UV−vis spectrum of hemin alone did not change during the course of a stopped-flow experiment. The fitting of kinetic data at 408 nm was performed using Origin 7.0. The first 100 ms of the H32A HasAp data was fitted to a single exponential, while the wt data were split into 0−40 ms and 0.04−4 s segments, each fitted to a single exponential to determine k_{1obs} and k_{2obs}, respectively. Amplitudes for the initial phase were fixed on the basis of the absorbance contribution of hemin before binding.

Rapid Freeze Quench (RFQ). Concentrations of apo-HasAp and hemin were determined as described above and were then diluted to ~1 mM in 200 mM HEPES (pH 7.5) and 10 mM NaOH, respectively. Solutions were then loaded into the System 1000 Chemical/Freeze Quench Apparatus (Update Instruments) equipped with a water bath maintained at 3−5 °C. We controlled reaction times by varying the syringe displacement rate from 2 to 8 cm/s or by varying the length of the reactor hose after the mixer. Five milliseconds were added to the calculated reaction times to account for time of flight and freezing in liquid ethane. Samples of 250 μL were ejected into a glass funnel attached to EPR or NMR tubes filled with liquid ethane at or below −120 °C. The frozen sample was packed into the tube as the assembly sat within a Teflon block cooled with liquid nitrogen to no higher than −100 °C. Liquid ethane was subsequently removed by immersing tubes in ethanol cooled to approximately −100 °C and applying vacuum for 5−10 min. RR analyses before and after cryosolvent removal showed no perturbation of spectra due to this treatment apart from the loss of bands originating from ethane. End point samples were generated by collecting reaction mixtures into a microcentrifuge tube and then transferring them to EPR tubes; 1:1 mixtures of buffer and 10 mM NaOH were checked to ensure that the final pH of RFQ samples remained near 7.5.

RR Spectroscopy. RR spectra were recorded using a custom McPherson 2061/207 spectrograph (0.67 m with variable gratings) equipped with a Princeton Instruments liquid N_2-cooled CCD detector (LN-1100PB). Excitation at 413 nm was provided by a krypton laser (Innova 302, Coherent), and a Kaiser Optical supernotch filter was used to attenuate Rayleigh scattering. Off-Soret excitations were provided by an argon laser (Innova 90, Coherent). Spectra at room temperature were recorded in a 90° scattering geometry on samples mounted on a reciprocating translation stage. Frequencies were calibrated relative to indene and CCl_4 and are accurate to ± 1 cm^{-1}. CCl_4 was also used to check the polarization conditions. The integrity of the RR samples, before and after laser illumination, was confirmed by direct monitoring of their UV−vis spectra in the Raman capillaries. Low-temperature spectra were recorded in a backscattering geometry on samples maintained at ~105 K in a liquid nitrogen coldfinger. Frequencies were calibrated relative to aspirin and are accurate to ± 1 cm^{-1}. Sodium selenate (Sigma) was chosen as an internal standard (*27*) and added at 100 mM (final concentration) to 500 μM samples of wt holo-HasAp, H32A holo-HasAp, and free hemin to determine their relative resonance enhancement based on the ν_4 intensity at 413 nm excitation and 105 K.

EPR Spectroscopy. EPR spectra were recorded on a Bruker E500 X-band EPR spectrometer equipped with a superX microwave bridge and a dual mode cavity with a helium-flow cryostat (ESR900, Oxford Instruments, Inc.). The experimental conditions, i.e., temperature, microwave power, and modulation amplitude, were varied to optimize the detection of all potential EPR active species and to ensure nonsaturating conditions. Known concentrations of wt and H32A holo-HasAp were used as standards to quantify low-spin (LS) (2300−4300 G) and high-spin (HS) (900−1900 G) signals, respectively, in RFQ samples by double integration. The signal intensity of a packed RFQ sample was typically ~75% of that of a hand-frozen sample of the same concentration, reflecting the density to which the frozen powders were packed.

RESULTS

Purification of apo-HasAp Proteins and Heme Acquisition from Hb. Expression of wild-type and H32A HasAp in *E. coli* produces a 1:4 mixture of holo- and apoprotein. While preparations of apo-HasAp by heme extraction in cold acid and acetone retain 1−5% holoproteins, hydrophobic affinity interaction columns allow complete separation of apo- and holo-HasAp. The absorption spectra of wt holo-HasAp and H32A holo-HasAp produced after reconstitution with hemin are shown

in Figure 1. These UV−vis spectra can be distinguished from that of human met-Hb at equivalent heme concentrations (Figure 1). Upon mixing wt apo-HasAp with met-Hb at a 4:1 apo-HasAp: heme ratio, we observed, over the course of 120 min, changes in the spectra consistent with unidirectional transport of ferric heme from Hb to HasAp (Figure 2). The change in absorbance at 618 nm was fitted to a double-exponential expression forced to have equal amplitudes, representing heme dissociation from α and β subunits (Figure 2). Observed rates of 4.0 and 0.6 h^{-1} were obtained from this analysis. These slow rates do not significantly deviate from literature values for the dissociation of ferric heme from the β and α subunits of human met-Hb (*14*, *28*).

These data support a mechanism of heme acquisition from met-Hb which relies on the dissociation of hemin from Hb and suggest that formation of a transient complex between wt apo-HasA and met-Hb may not influence the heme dissociation rate.

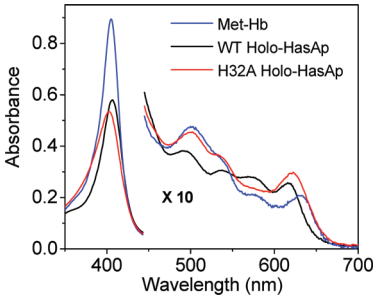

FIGURE 1: Absorption spectra of human met-Hb (blue), wt holo-HasAp (black), and H32A holo-HasAp (red) normalized to 5.0 μM heme.

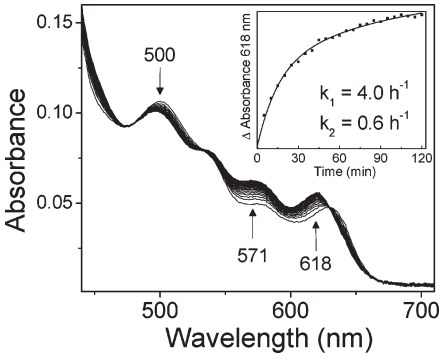

FIGURE 2: Absorption spectra of human met-Hb (50 μM heme) combined with 200 μM wt apo-HasAp at room temperature and pH 7.0. Solutions were loaded in a 2 mm cuvette, and scans were taken every 5 min. Arrows show the direction of change over time. The inset shows the absorbance change at 618 nm vs time (scattered points) and a double-exponential fit (solid line).

As expected, wt apo-HasAp is unable to acquire heme over the course of 2 h from either reduced Hb, where heme dissociation is precluded, or met-myoglobin, where the dissociation rate is extremely slow (0.01 h^{-1}) (*14*) (data not shown).

HasAp Hemin Binding. The much more rapid binding of free hemin to apo-HasAp required monitoring by stopped-flow spectroscopy at 4 °C. The concentration ratio of hemin to apo-HasAp was kept low (< 0.25) to maintain pseudo-first-order conditions. Mixing hemin with excess wt apo-HasAp results in a rapid increase in absorbance at 403 nm followed by a more gradual increase in absorbance and red shift to 408 nm (ε_{408} = 116 mM^{-1} cm^{-1}) that corresponds to the Soret absorption maximum of wt holo-HasAp (Figure 3A). This second phase of the reaction is characterized in the 450−700 nm range of the spectra by a diminution in absorbance at 622 nm and a growth at 570 nm, consistent with the partial conversion of heme iron(III) from HS to LS (*29*). When the same experiment is performed with H32A apo-HasAp, only the initial rapid phase is observed, with a growth in absorbance at 403 nm (ε_{403} = 106 mM^{-1} cm^{-1}) (Figure 3B); in the 450−700 nm range, where absorption maxima from hemin and H32A holo-HasAp are similar, an overall increase in absorbance is observed. Control experiments with hemin in the absence of HasAp confirm that no spectral changes occur on this time scale after mixing with the buffer blank (blue traces, Figure 3A,B). Of particular interest is the fact that the absorption changes observed upon mixing hemin with the wt and variant proteins are essentially the same in the first 20 ms (red traces, Figure 3A,B), after which only the wt protein exhibits the onset of a second phase (black traces, Figure 3A,B). Indeed, the 20 ms absorption spectrum of the heme binding reaction with wt HasAp is nearly identical to that of H32A HasAp after 20 ms and beyond (Figure 3C), which suggests similar heme coordination environments in the transient complex of wt HasAp and the resting H32A variant holoprotein.

The kinetics measured at 408 nm clearly illustrate that hemin binding by wt apo-HasAp is biphasic with a fast rate (k_{1obs}) and a slow rate (k_{2obs}), while the H32A mutant binds hemin in a single rapid step (k_{1obs}) (Figure 4A). Measurements at different apo-HasAp concentrations yield similar k_{1obs} values for wt and H32A HasAp, with a hyperbolic dependence of k_{1obs} on apo-HasAp concentration (Figure 4B). The slower phase k_{2obs}, observed only with wt apo-HasAp, exhibits no significant dependence on apo-HasAp concentration and has an average value of 5.3 ± 0.6 s^{-1} at 4 °C.

The hyperbolic dependence of hemin binding rates on apo-protein concentration has been successfully modeled by a two-step process for a number of hemoproteins (*23*, *30*). It includes the formation of a hemin−apoprotein reversible complex, within

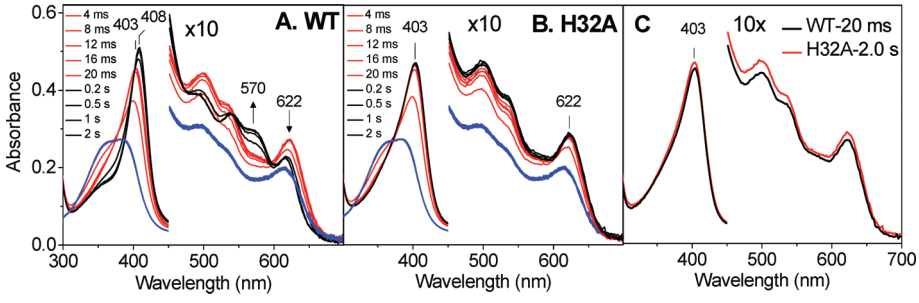

FIGURE 3: Stopped-flow absorption spectra of the association of 4.45 μM hemin with (A) wt and (B) H32A apo-HasAp at 31 μM. Blue traces are hemin/buffer controls at the same times as those indicated for the proteins. (C) Comparison between the absorption spectra of the intermediate obtained 20 ms after mixing of hemin with wt apo-HasAp (black) and 2.0 s after mixing of hemin with H32A holo-HasAp (red).

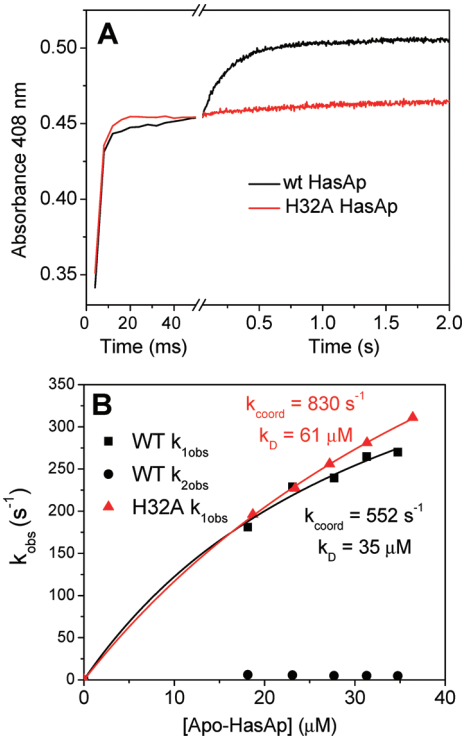

FIGURE 4: (A) Kinetics of hemin association measured at 408 nm for wt (black) and H32A (red) HasAp. (B) Observed rate constants plotted as a function of apo-HasAp concentration for wt (black) and H32A (red) HasAp as determined by single-exponential fitting of the 408 nm absorbance.

Scheme 1

$$\text{Apoprotein} + \text{hemin} \underset{k_2}{\overset{k_1}{\rightleftharpoons}} \text{Apoprotein-hemin} \underset{k_{-\text{hemin}}}{\overset{k_{coord}}{\rightleftharpoons}} \text{Holoprotein}$$

the mixing time of the experiment and prior to iron coordination (Scheme 1) (*23*, *30*). Relying on the assumption that k_1[apoprotein] and $k_2 \gg k_{coord} \gg k_{-hemin}$, we can fit the dependence of k_{1obs} on the concentration of apo-HasAp using eq 1.

$$\begin{aligned} k_{1obs} &= k_{coord}[\text{apoprotein}]/[(k_2 + k_{coord})/k_1 + [\text{apoprotein}]] \\ &\approx k_{coord}[\text{apoprotein}]/K_d + [\text{apoprotein}] \end{aligned} \quad (1)$$

This model can be used to analyze the rapid first phase of hemin binding to wt apo-HasAp (k_{1obs}) prior to the onset of k_{2obs}. This analysis yields k_{coord} and K_d values of 552 s^{-1} and 35 μM for wt apo-HasAp and 830 s^{-1} and 61 μM for H32A apo-HasAp, respectively. In turn, these values lead to apparent bimolecular rate constants k'_{hemin} ($\approx k_{coord}/K_d$) of 16 and 14 μM^{-1} s^{-1} for wt and H32A HasAp, respectively. Because these initial binding steps are very rapid, even at 4 °C, and only a few points are available to determine k_{1obs} values (Figure 4A), these kinetic parameters should be viewed as evidence of conserved characteristics of hemin binding in wt and H32A HasAp proteins, as well as in other heme acquisition proteins (Table 1) (*23*, *30*, *31*). Thus, the data suggest a model for hemin binding to wt apo-HasAp where the first observable step is the rapid coordination of the heme iron to Tyr75 with accumulation of an intermediate species closely resembling H32A HasAp. This first coordination step is followed by a second step, only observed with wt HasAp and independent of the protein concentration, which corresponds to the binding of the His32 ligand to the heme iron(III) and the closing of the His32 loop to complete the heme binding pocket.

To better characterize the heme-binding intermediate in wt HasAp, the reactions of hemin with both wt and H32A apo-HasAp were rapidly freeze quenched (RFQ) at 7, 21, 100, and 500 ms for EPR and RR analyses. EPR spectra of RFQ samples of wt HasAp reveal a conversion from HS to LS ferric heme which is essentially complete by 500 ms (Figure 5A).[2] The HS $g = 6$ signal is composed of multiple resonances with major $g = 6.09$ and 5.62 signals and smaller $g = 6.69$ and 5.13 features. The minor signals cannot be assigned to free hemin, which shows very weak EPR signals in control experiments, presumably because of significant antiferromagnetic coupling between iron(III) centers in hemin-stacked dimers (Figure S1 of the Supporting Information). EPR spectra of RFQ samples of H32A HasAp exhibit the same major and minor $g \sim 6$ resonances, but the conversion to LS is not observed (Figure 5B). In both proteins, the minor $g = 6.69$ and 5.13 resonances disappear after 100 ms (Figure 5A,B). Double integrations of the $g \sim 2$ and $g \sim 6$ regions of the EPR spectra of reconstituted wt and H32A holo-HasAp samples allow for quantification of the relative abundance of LS and HS species in the RFQ samples of wt HasAp (see Materials and Methods). This analysis produces an apparent rate of conversion for the HS intermediate to the LS resting state of 9.0 s^{-1} (Figure 5C), in good agreement with the k_{2obs} of 5.3 s^{-1} deduced from the UV−vis stopped-flow data.

The same RFQ samples were also characterized by RR spectroscopy. High-frequency RR spectra of heme proteins obtained with Soret excitation are diagnostic of the heme-iron status, with the porphyrin skeletal mode ν_4 correlating with the oxidation state of the iron, and the ν_3, ν_2, and ν_{10} modes reporting on the iron coordination and spin states (*32*). The RR spectra of the RFQ samples trapped within 7 ms are mixtures of six-coordinate high-spin (6cHS) and five-coordinate high-spin (5cHS) species as indicated by the presence of ν_3 modes at 1479 and 1489 cm^{-1}, respectively (Figure 6A,B). Over time, this species is converted to a predominantly six-coordinate low-spin (6cLS) product in wt HasAp, as shown by the growth of ν_3 at 1504 cm^{-1} concurrent with the disappearance of the other ν_3 modes (Figure 6A). It should be noted that the spin state of wt holo-HasAp is temperature-dependent, with 6cHS to 6cLS conversion occurring with decreasing temperature (Figure S2 of the Supporting Information). Thus, although the EPR spectrum at 7.4 K suggests an essentially pure 6cLS heme in wt holo-HasAp, the RR spectrum of the same species at 105 K indicates the presence of some 6cHS. In comparison, the RR spectra of H32A HasAp RFQ samples show relatively little change over time (Figure 6B). The mixture of 6cHS and 5cHS species observed in the 7 ms RFQ sample with H32A evolves only slightly with time to favor the 6cHS coordination, and this transformation appears to be largely completed within 100 ms (Figure 6B). This decay in 5cHS signals in the RR spectra seems to correlate with that of the minor EPR $g = 6.69$ and 5.13 resonances (Figure 5). The RR spectra of RFQ samples with long reaction times and those of reconstituted H32A HasAp are undistinguishable, but it is important to make the comparison at the same temperature since the RR spectra of H32A holo-HasAp are temperature sensitive, exhibiting an increase in

[2]Our earlier EPR analyses of wt HasAp (*15*) revealed approximately 15% high-spin ferric heme contributions, but the improved purification procedure used here to isolate the apo form leads to high-spin contributions of no more than 5% after hemin reconstitution.

Table 1: Kinetic Parameters for Hemin Binding to wt and Mutant Heme Acquisition Proteins

	hemophore (room-temperature coordination of the resting holo form)					
kinetic parameter	wt HasAp[a,b] (6cHS/LS)	H32A HasAp[a,b] (5cHS/6cHS)	wt HtsA[c] (6cLS)	wt Shp[c] (6cLS)	M153A Shp[d] (5cHS)	wt IsdA[e] (5cHS)
K_d (μM)	35	61	8 ± 0.7	22 ± 2	62 ± 7	3.3 ± 0.7
k_{coord} (s^{-1})	552	830	655 ± 47	35 ± 4	490 ± 24	330 ± 27
k'_{hemin} (μM^{-1} s^{-1})	16	14	80	1.6	7.9	100
k_{2obs} (s^{-1})	5.3 ± 0.6[f]	not observed	not observed	not observed	not observed	not observed

[a]This work from measurements taken at 4 °C. [b]Affinity constants for the binding of hemin to wt and H32A HasAm have been measured by displacement isothermal titration calorimetry at 25 °C in ref *2*. [c]From measurements at 25 °C (*23*). [d]From measurements at 25 °C (*31*). [e]From measurements at 25 °C (*30*). [f]Standard deviation from five measurements at different HasAp concentrations.

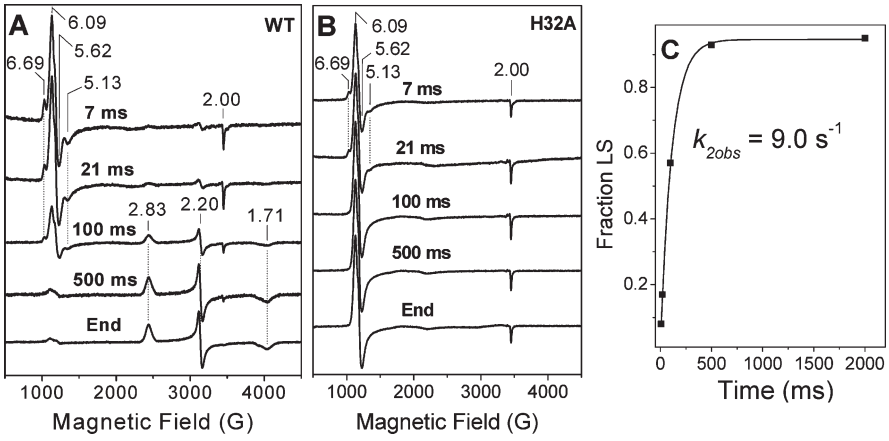

FIGURE 5: X-Band EPR spectra of RFQ samples of the reaction of 1 equiv of hemin with (A) wt and (B) H32A apo-HasAp at 760 and 950 μM, respectively. Spectra are normalized according to double integrations of EPR signals from known concentrations of holo-HasAp (see Materials and Methods) (0.0317 mW microwave power, 10 G modulation amplitude, 7.4 K). (C) Quantification of the relative concentration of LS heme in hemin/wt apo-HasAp RFQ samples and fit to a single exponential.

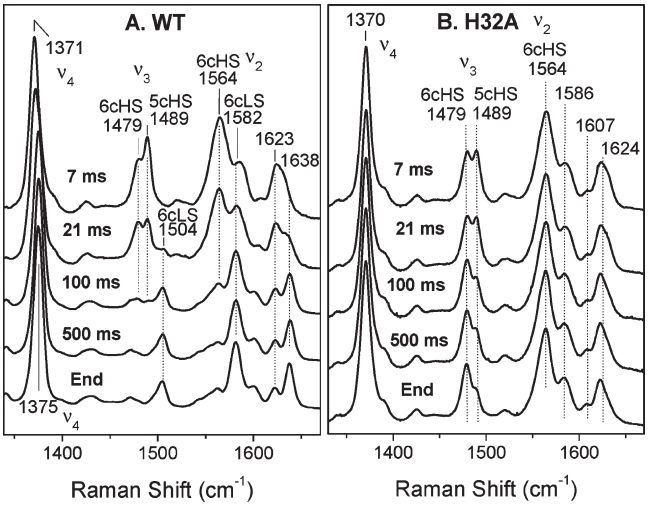

FIGURE 6: High-frequency RR spectra of RFQ samples of the reaction of 1 equiv of hemin with (A) wt and (B) H32A apo-HasAp at 760 and 950 μM, respectively (λ_{exc} = 413 nm, 20 mW; all spectra are normalized on the intensity of the ν_4 feature observed between 1370 and 1375 cm^{-1}).

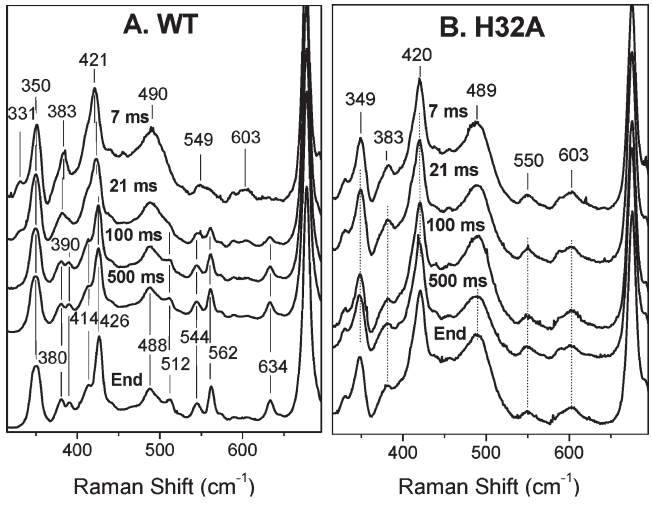

FIGURE 7: Low-frequency RR spectra of RFQ samples of the reaction of 1 equiv of hemin with (A) wt and (B) H32A apo-HasAp at 760 and 950 μM, respectively (λ_{exc} = 413 nm, 20 mW; all spectra are normalized on the intensity of the ν_7 feature observed between 676 and 677 cm^{-1}).

the level of 6cHS components with a decrease in temperature (Figure S2 of the Supporting Information).

The low-frequency region of the RR spectra of RFQ samples from H32A shows no significant changes for different reaction times (Figure 7B). A RR band at 489 cm^{-1} is a close match for the 491 cm^{-1} HS ν(Fe−OH) feature of alkaline met-Mb (*33*); however, this feature is not sensitive to solvent exchange with D_2O and $H_2{}^{18}O$ (data not shown), leading us to speculate that the sixth ligand in these H32A samples is an aqua ligand. The low-frequency RR spectrum of the 7 ms RFQ sample of the wt protein is nearly identical to that of H32A HasAp, while that of the 500 ms RFQ sample is nearly indistinguishable from that of the resting wt protein (Figure 7A). The sharp RR bands at 544, 562, and 634 cm^{-1} are likely to correspond to out-of-plane

pyrrole vibrations, while bands at ~380 and 426 cm^{-1} include significant contributions from out-of-plane modes of peripheral substituents (*34*−*37*).

RR spectra were also recorded with a 514 nm excitation as Q-band excitations have been shown to enhance phenolate vibrations in several tyrosinate ligated ferric heme proteins (*38*−*43*). However, these experiments did not reveal RR bands that could be assigned to phenolate vibrations in the HS intermediate trapped in wt HasAp or in the H32A variant (data not shown). Earlier efforts by us and others (*44*) to identify tyrosinate RR vibrations in resting ferric HasA wt and variant proteins were equally unsuccessful.

DISCUSSION

The mechanisms by which hemophores are used by pathogenic bacteria to acquire iron from the host are of considerable interest given their apparent role in virulence. The observation of transient complex formation between met-Hb and holo-HasAp (*15*) suggested that specific interactions between these proteins may predispose apo-HasAp to this large reservoir of heme and facilitate its extraction. However, our kinetic study shows no evidence of an increase in the rate of dissociation of hemin from Hb upon the addition of apo-HasAp and thus suggests that, although apo-HasAp is capable of acquiring heme from met-Hb, it may do so by simply scavenging dissociated hemin. This mechanism could be sufficient given the relatively rapid dissociation of hemin from met-Hb at low concentrations (*14*), a condition that is likely to be relevant in vivo upon erythrocyte lysis. Moreover, apo-HasAp may actively target other host hemoproteins such as albumin or hemopexin; experiments to explore these possibilities are currently underway in our laboratories.

The second part of our investigation sought to characterize the mechanism by which apo-HasAp acquires free hemin. The mechanism of hemin binding to apo-HasAp is proposed to involve its initial coordination to Tyr75 followed by closing of the His32 loop and His32 coordination (*19*), but until now, kinetic parameters and spectroscopic evidence for this two-step binding mechanism were lacking. Alternative mechanisms can be envisioned, including initial coordination by His32 or simultaneous coordination by both axial ligands. We used rapid spectroscopic techniques on both wt and H32A apo-HasAp in an attempt to describe the binding of hemin in solution.

Our stopped-flow experiments showed that hemin binding to wt apo-HasAp proceeds in two distinct phases via the formation of a HS intermediate, whereas H32A apo-HasAp binds hemin in a single rapid step. Completion of the first phase of hemin binding to wt apo-HasAp occurs within a few milliseconds and results in the buildup of an intermediate whose UV−vis spectrum closely matches that of H32A holo-HasAp. Kinetic parameters for this initial binding phase correspond to a combination of two components, a bimolecular association and a first heme coordination event, and are essentially the same in the wt and variant proteins (Table 1). The second phase observed only with wt HasAp is relatively slow with a k_{2obs} of ~5 s^{-1} at 4 °C and suggests a conversion of the HS intermediate species to a LS species, as observed in wt holo-HasAp (Figure S2 of the Supporting Information). Because this second phase is not observed with H32A-HasAp, it is reasonable to propose that this step represents the closing of the His32 loop and coordination of the heme iron by His32.

Kinetic analyses of hemin binding to proteins are potentially complicated by the presence of hemin dimers in aqueous solution. Dimers are stabilized by noncovalent $\pi-\pi$ stacking interactions and exist even at very low hemin concentrations with a dimerization constant K_{dimer} of ~6 μM^{-1} at pH 7.5 (*45*). An aqueous hemin monomer−dimer equilibrium has been proposed to be the source of biphasic rates of kinetic binding of hemin to the iron-regulated surface determinant protein IsdA of *Staphylococcus aureus* (*30*); the fast phase was assigned to hemin monomer binding, and the slow phase, which was independent of the apo-IsdA concentration, was to represent hemin−dimer dissociation. However, stopped-flow experiments with H32A apo-HasAp do not reveal any evidence of biphasic binding kinetics, suggesting that the hemin monomer−dimer conversion rates are extremely rapid and do not affect the observed rates of hemin binding to wt and H32A HasAp. Stopped-flow experiments performed at different hemin concentrations in an effort to vary the hemin monomer−dimer distribution did not affect the kinetic data.[3]

RR and EPR characterization of our RFQ samples support the interpretation of the stopped-flow UV−vis data and also provide interesting additional details. The RFQ samples obtained with H32A HasAp show minor changes in the high-frequency RR spectra over the first 100 ms, with a loss of 5cHS contributions relative to 6cHS signals (Figure 6B); these changes seem to correlate with the loss of $g = 6.69$ and 5.13 resonances in the EPR spectra (Figure 5B). Similar early changes in the RR and EPR spectra are observed in the RFQ samples of wt-HasAp; these features do not match those of free hemin controls (Figure S1 of the Supporting Information), and they are not replicated by reconstitution of HasAp with excess hemin or by altering the pH of H32A holo-HasAp between 6.0 and 9.2 (data not shown). Thus, these spectral features are unlikely to originate from a second adventitious hemin binding site, and they may instead identify a precursor to resting H32A holo-HasAp. Hemin may bind to HasAp initially as a 5cHS species before coordination of a solvent molecule to form a 6cHS species, but other interpretations exist. RR experiments in D_2O or $H_2{}^{18}O$ solvent did not identify iron(III)−$O_{solvent}$ stretching vibrations, but such modes are rarely observed except in the case of hydroxide ligands. Although direct identification of iron(III)−axial ligand vibrations could not be obtained from the RR analysis, the similarities of the UV−vis, EPR, and RR spectra of the wt HS intermediate and H32A holo-HasAp provide strong support for a conserved heme iron(III) coordination by Tyr75 in these two heme−protein complexes. Our recent structural investigation of H32A holo-HasAp supports this conclusion (*16*).

The relatively slow rate associated with the closing of the H32 loop on the heme binding site ($t_{1/2}$ ~ 140 ms at 4 °C) of wt-HasAp

[3]Stopped-flow analyses of heme uptake in wt and H32A apoproteins with starting hemin concentrations between 30 and 40 μM show absorption traces and kinetic behaviors that are qualitatively equivalent to measurements taken at heme concentrations one tenth of these. Since the vast majority of hemin is expected to be dimerized, a slow heme monomer−dimer equilibrium could lead to the formation of heme-containing stack HasAp dimers. However, the absorption spectra observed 20 ms after mixing for wt and H32A HasAp are identical to those of monomeric H32A holo-HasAp, with no evidence of broadening or weakening of the Soret absorption. This point is noteworthy because dimerization of HasA systems is known to occur. Specifically, wt holo-HasAs dimer with domain swapping between subunits has been characterized by X-ray crystallography (*49*). Also, H32A-HasAp can form holodimers with each subunit binding one heme to Tyr75 (*16*). In this structure, the two hemes are stacked, and in solution, this interaction results in a distinct weakening and broadening of the heme Soret absorptions (data not shown).

is consistent with crystal and solution structures of the apoprotein in which the H32 loop is flipped away from the heme binding site (*16*, *19*). The low-frequency RR spectra of wt and H32A holoproteins exhibit marked differences in pyrrole and peripheral group out-of-plane deformation modes and may reflect increased out-of-plane porphyrin deformation in the wt protein upon formation of hydrogen bonds between heme propionates and residues located on the His32 loop, as observed in the crystal structures of both HasAs and HasAp (*15*, *17*, *19*). Important to this study, the RR spectra of the RFQ samples of wt HasAp do not reveal any conformational states other than the "H32A-like" intermediate and the wt holo-HasAp complex. Indeed, the RFQ experiments do not kinetically resolve the formation of the iron(III)−N(His32) bond, which results in the HS to LS transition, from the changes in low-frequency modes that primarily reflect interactions between the His32 loop and heme peripheral groups.

In conclusion, our kinetic studies of heme acquisition by apo-HasAp from met-Hb show that apo-HasAp scavenges dissociated hemin from met-Hb via a passive mechanism. Time-resolved analyses of free hemin acquisition by apo-HasAp reveal a near stoichiometric buildup of a millisecond intermediate that can be trapped using RFQ techniques. The intermediate shows striking spectral similarities with the variant H32A holo-HasAp, supporting the idea of iron(III) ligation by Tyr75 as the initial step in the binding of hemin to HasAp. Conversion of this HS intermediate to the LS state seen in wt holo-HasA occurs, without the appearance of other intermediate species, with a first-order rate of 5 s^{-1} at 4 °C. This second phase in the formation of wt holo-HasAp is assigned to the closing of the H32 loop, leading to further stabilization of the heme−protein complex. This loop motion is expected to be facilitated by two hinge regions consisting of Phe27 and Gly28 and of Gly43, Gly44, and Phe45 (*16*, *19*), but while similar protein dynamics have been shown to occur in the nanosecond to millisecond range (*46*−*48*), the rate of closure of the H32 loop in HasAp is slow. This slow rate is consistent with the large number of contacts between the H32 loop and the apoprotein core (*16*, *19*), and it does not support an induced-fit process based on a rapid dynamic equilibrium between open and closed configurations of the H32 loop prior to heme capture. Instead, the data indicate that binding of hemin to Tyr75 must be established before the His32 loop can sample its closed configuration. Time-resolved spectroscopic studies, as reported here, will be useful for testing proposals from molecular dynamics-based models of the sequence of events leading to the closure of the H32 loop on the bound high-spin ferric heme in HasAp (*16*).

SUPPORTING INFORMATION AVAILABLE

EPR spectrum of the control RFQ sample of hemin and buffer and RR spectra of wt and H32A HasAp at room temperature and 105 K. This material is available free of charge via the Internet at http://pubs.acs.org.

REFERENCES

1. Letoffe, S., Ghigo, J. M., and Wandersman, C. (1994) Iron acquisition from heme and hemoglobin by a *Serratia marcescens* extracellular protein. *Proc. Natl. Acad. Sci. U.S.A. 91*, 9876–9880.
2. Deniau, C., Gilli, R., Izadi-Pruneyre, N., Letoffe, S., Delepierre, M., Wandersman, C., Briand, C., and Lecroisey, A. (2003) Thermodynamics of heme binding to the HasA(SM) hemophore: Effect of mutations at three key residues for heme uptake. *Biochemistry 42*, 10627–10633.
3. Ghigo, J. M., Letoffe, S., and Wandersman, C. (1997) A new type of hemophore-dependent heme acquisition system of *Serratia marcescens* reconstituted in *Escherichia coli*. *J. Bacteriol. 179*, 3572–3579.
4. Ratliff, M., Zhu, W., Deshmukh, R., Wilks, A., and Stojiljkovic, I. (2001) Homologues of neisserial heme oxygenase in gram-negative bacteria: Degradation of heme by the product of the pigA gene of *Pseudomonas aeruginosa*. *J. Bacteriol. 183*, 6394–6403.
5. Berka, R. M., and Vasil, M. L. (1982) Phospholipase C (heat-labile hemolysin) of *Pseudomonas aeruginosa*: Purification and preliminary characterization. *J. Bacteriol. 152*, 239–245.
6. Pritchard, A. E., and Vasil, M. L. (1986) Nucleotide sequence and expression of a phosphate-regulated gene encoding a secreted hemolysin of *Pseudomonas aeruginosa*. *J. Bacteriol. 167*, 291–298.
7. Vasil, M. L., Kabat, D., and Iglewski, B. H. (1977) Structure-activity relationships of an exotoxin of *Pseudomonas aeruginosa*. *Infect. Immun. 16*, 353–361.
8. Letoffe, S., Redeker, V., and Wandersman, C. (1998) Isolation and characterization of an extracellular haem-binding protein from *Pseudomonas aeruginosa* that shares function and sequence similarities with the *Serratia marcescens* HasA haemophore. *Mol. Microbiol. 28*, 1223–1234.
9. Letoffe, S., Nato, F., Goldberg, M. E., and Wandersman, C. (1999) Interactions of HasA, a bacterial haemophore, with haemoglobin and with its outer membrane receptor HasR. *Mol. Microbiol. 33*, 546–555.
10. Cescau, S., Cwerman, H., Letoffe, S., Delepelaire, P., Wandersman, C., and Biville, F. (2007) Heme acquisition by hemophores. *Biometals 20*, 603–613.
11. Turner, G. J., Galacteros, F., Doyle, M. L., Hedlund, B., Pettigrew, D. W., Turner, B. W., Smith, F. R., Moo-Penn, W., Rucknagel, D. L., and Ackers, G. K. (1992) Mutagenic dissection of hemoglobin cooperativity: Effects of amino acid alteration on subunit assembly of oxy and deoxy tetramers. *Proteins 14*, 333–350.
12. Benesch, R. E., and Kwong, S. (1995) Coupled reactions in hemoglobin. Heme-globin and dimer-dimer association. *J. Biol. Chem. 270*, 13785–13786.
13. Zhang, L., Levy, A., and Rifkind, J. M. (1991) Autoxidation of hemoglobin enhanced by dissociation into dimers. *J. Biol. Chem. 266*, 24698–24701.
14. Hargrove, M. S., Whitaker, T., Olson, J. S., Vali, R. J., and Mathews, A. J. (1997) Quaternary structure regulates hemin dissociation from human hemoglobin. *J. Biol. Chem. 272*, 17385–17389.
15. Alontaga, A. Y., Rodriguez, J. C., Schonbrunn, E., Becker, A., Funke, T., Yukl, E. T., Hayashi, T., Stobaugh, J., Moënne-Loccoz, P., and Rivera, M. (2009) Structural characterization of the hemophore HasAp from *Pseudomonas aeruginosa*: NMR spectroscopy reveals protein-protein interactions between Holo-HasAp and hemoglobin. *Biochemistry 48*, 96–109.
16. Jepkorir, G., Rodriguez, J. C., Rui, H., Im, W., Lovell, S., Battaile, K. P., Alontaga, A. Y., Yukl, E. T., Moënne-Loccoz, P., and Rivera, M. (2010) Structural, NMR spectroscopy and computational investigation of hemin loading in the hemophore HasAp from *Pseudomonas aeruginosa*. *J . Am. Chem. Soc. 132*, 9857–9872.
17. Arnoux, P., Haser, R., Izadi, N., Lecroisey, A., Delepierre, M., Wandersman, C., and Czjzek, M. (1999) The crystal structure of HasA, a hemophore secreted by *Serratia marcescens*. *Nat. Struct. Biol. 6*, 516–520.
18. Arnoux, P., Haser, R., Izadi-Pruneyre, N., Lecroisey, A., and Czjzek, M. (2000) Functional aspects of the heme bound hemophore HasA by structural analysis of various crystal forms. *Proteins 41*, 202–210.
19. Wolff, N., Izadi-Pruneyre, N., Couprie, J., Habeck, M., Linge, J., Rieping, W., Wandersman, C., Nilges, M., Delepierre, M., and Lecroisey, A. (2008) Comparative analysis of structural and dynamic properties of the loaded and unloaded hemophore HasA: Functional implications. *J. Mol. Biol. 376*, 517–525.
20. Rossi, M. S., Fetherston, J. D., Letoffe, S., Carniel, E., Perry, R. D., and Ghigo, J. M. (2001) Identification and characterization of the hemophore-dependent heme acquisition system of *Yersinia pestis*. *Infect. Immun. 69*, 6707–6717.
21. Lukat-Rodgers, G. S., Rodgers, K. R., Caillet-Saguy, C., Izadi-Pruneyre, N., and Lecroisey, A. (2008) Novel heme ligand displacement by CO in the soluble hemophore HasA and its proximal ligand mutants: Implications for heme uptake and release. *Biochemistry 47*, 2087–2098.
22. Krieg, S., Huche, F., Diederichs, K., Izadi-Pruneyre, N., Lecroisey, A., Wandersman, C., Delepelaire, P., and Welte, W. (2009) Heme uptake across the outer membrane as revealed by crystal structures of the receptor-hemophore complex. *Proc. Natl. Acad. Sci. U.S.A. 106*, 1045–1050.

23. Nygaard, T. K., Blouin, G. C., Liu, M., Fukumura, M., Olson, J. S., Fabian, M., Dooley, D. M., and Lei, B. (2006) The mechanism of direct heme transfer from the streptococcal cell surface protein Shp to HtsA of the HtsABC transporter. *J. Biol. Chem. 281*, 20761–20771.
24. Ran, Y., Liu, M., Zhu, H., Nygaard, T. K., Brown, D. E., Fabian, M., Dooley, D. M., and Lei, B. (2010) Spectroscopic identification of heme axial ligands in HtsA that are involved in heme acquisition by *Streptococcus pyogenes*. *Biochemistry 49*, 2834–2842.
25. Aranda, R., IV, Worley, C. E., Liu, M., Bitto, E., Cates, M. S., Olson, J. S., Lei, B., and Phillips, G. N., Jr. (2007) Bis-methionyl coordination in the crystal structure of the heme-binding domain of the streptococcal cell surface protein Shp. *J. Mol. Biol. 374*, 374–383.
26. Dawson, R. M. C., Elliott, D. C., Elliott, W. H., and Jones, K. M. (1986) in Data for Biochemical Research, pp 230−231, Oxford University Press, Oxford, England.
27. Song, S. H., and Asher, S. A. (1991) Internal intensity standards for heme protein UV resonance Raman studies: Excitation profiles of cacodylic acid and sodium selenate. *Biochemistry 30*, 1199–1205.
28. Zhu, H., Xie, G., Liu, M., Olson, J. S., Fabian, M., Dooley, D. M., and Lei, B. (2008) Pathway for heme uptake from human methemoglobin by the iron-regulated surface determinants system of *Staphylococcus aureus*. *J. Biol. Chem. 283*, 18450–18460.
29. Makinen, M. W., and Churg, A. K. (1983) in Iron Porphyrins (Lever, A. B. P., and Gray, H. B., Eds.) pp 141−236, Addison-Wesley Publishing Co., Reading, MA.
30. Liu, M., Tanaka, W. N., Zhu, H., Xie, G., Dooley, D. M., and Lei, B. (2008) Direct hemin transfer from IsdA to IsdC in the iron-regulated surface determinant (Isd) heme acquisition system of *Staphylococcus aureus*. *J. Biol. Chem. 283*, 6668–6676.
31. Ran, Y., Zhu, H., Liu, M., Fabian, M., Olson, J. S., Aranda, R., IV, Phillips, G. N., Jr., Dooley, D. M., and Lei, B. (2007) Bis-methionine ligation to heme iron in the streptococcal cell surface protein Shp facilitates rapid hemin transfer to HtsA of the HtsABC transporter. *J. Biol. Chem. 282*, 31380–31388.
32. Spiro, T. G., and Li, X. Y. (1988) in Biological Applications of Raman Spectroscopy. Vol. 3. Resonance Raman spectra of hemes and metalloproteins (Spiro, T. G., Ed.) pp 1−37, John Wiley & Sons, New York.
33. Feis, A., Marzocchi, M. P., Paoli, M., and Smulevich, G. (1994) Spin state and axial ligand bonding in the hydroxide complexes of metmyoglobin, methemoglobin, and horseradish peroxidase at room and low temperatures. *Biochemistry 33*, 4577–4583.
34. Hu, S., Smith, K. M., and Spiro, T. G. (1996) Assignment of protoheme resonance Raman spectrum by heme labeling in myoglobin. *J. Am. Chem. Soc. 118*, 12638–12646.
35. Peterson, E. S., Friedman, J. M., Chien, E. Y., and Sligar, S. G. (1998) Functional implications of the proximal hydrogen-bonding network in myoglobin: A resonance Raman and kinetic study of Leu89, Ser92, His97, and F-helix swap mutants. *Biochemistry 37*, 12301–12319.
36. Mak, P. J., Podstawka, E., Kincaid, J. R., and Proniewicz, L. M. (2004) Effects of systematic peripheral group deuteration on the low-frequency resonance Raman spectra of myoglobin derivatives. *Biopolymers 75*, 217–228.
37. Mak, P. J., Kaluka, D., Manyumwa, M. E., Zhang, H., Deng, T., and Kincaid, J. R. (2008) Defining resonance Raman spectral responses to substrate binding by cytochrome P450 from *Pseudomonas putida*. *Biopolymers 89*, 1045–1053.
38. Nagai, M., Yoneyama, Y., and Kitagawa, T. (1989) Characteristics in tyrosine coordinations of four hemoglobins M probed by resonance Raman spectroscopy. *Biochemistry 28*, 2418–2422.
39. Egeberg, K. D., Springer, B. A., Martinis, S. A., Sligar, S. G., Morikis, D., and Champion, P. M. (1990) Alteration of sperm whale myoglobin heme axial ligation by site-directed mutagenesis. *Biochemistry 29*, 9783–9791.
40. Adachi, S., Nagano, S., Ishimori, K., Watanabe, Y., Morishima, I., Egawa, T., Kitagawa, T., and Makino, R. (1993) Roles of proximal ligand in heme proteins: replacement of proximal histidine of human myoglobin with cysteine and tyrosine by site-directed mutagenesis as models for P-450, chloroperoxidase, and catalase. *Biochemistry 32*, 241–252.
41. Liu, Y., Moënne-Loccoz, P., Hildebrand, D. P., Wilks, A., Loehr, T. M., Mauk, A. G., and Ortiz de Montellano, P. R. (1999) Replacement of the proximal histidine iron ligand by a cysteine or tyrosine converts heme oxygenase to an oxidase. *Biochemistry 38*, 3733–3743.
42. Jin, Y., Nagai, M., Nagai, Y., Nagatomo, S., and Kitagawa, T. (2004) Heme structures of five variants of hemoglobin M probed by resonance Raman spectroscopy. *Biochemistry 43*, 8517–8527.
43. Eakanunkul, S., Lukat-Rodgers, G. S., Sumithran, S., Ghosh, A., Rodgers, K. R., Dawson, J. H., and Wilks, A. (2005) Characterization of the periplasmic heme-binding protein shut from the heme uptake system of *Shigella dysenteriae*. *Biochemistry 44*, 13179–13191.
44. Caillet-Saguy, C., Turano, P., Piccioli, M., Lukat-Rodgers, G. S., Czjzek, M., Guigliarelli, B., Izadi-Pruneyre, N., Rodgers, K. R., Delepierre, M., and Lecroisey, A. (2008) Deciphering the structural role of histidine 83 for heme binding in hemophore HasA. *J. Biol. Chem. 283*, 5960–5970.
45. de Villiers, K. A., Kaschula, C. H., Egan, T. J., and Marques, H. M. (2007) Speciation and structure of ferriprotoporphyrin IX in aqueous solution: Spectroscopic and diffusion measurements demonstrate dimerization, but not μ-oxo dimer formation. *J. Biol. Inorg. Chem. 12*, 101–117.
46. Waldman, A. D., Hart, K. W., Clarke, A. R., Wigley, D. B., Barstow, D. A., Atkinson, T., Chia, W. N., and Holbrook, J. J. (1988) The use of genetically engineered tryptophan to identify the movement of a domain of *B. stearothermophilus* lactate dehydrogenase with the process which limits the steady-state turnover of the enzyme. *Biochem. Biophys. Res. Commun. 150*, 752–759.
47. Nicholson, L. K., Yamazaki, T., Torchia, D. A., Grzesiek, S., Bax, A., Stahl, S. J., Kaufman, J. D., Wingfield, P. T., Lam, P. Y., Jadhav, P. K., Hodge, C. N., Domaille, P. J., and Chang, C.-H. (1995) Flexibility and function in HIV-1 protease. *Nat. Struct. Biol. 2*, 274–280.
48. Gulotta, M., Deng, H., Dyer, R. B., and Callender, R. H. (2002) Toward an understanding of the role of dynamics on enzymatic catalysis in lactate dehydrogenase. *Biochemistry 41*, 3353–3363.
49. Czjzek, M., Letoffe, S., Wandersman, C., Delepierre, M., Lecroisey, A., and Izadi-Pruneyre, N. (2007) The Crystal Structure of the Secreted Dimeric Form of the Hemophore HasA Reveals a Domain Swapping with an Exchanged Heme Ligand. *J. Mol. Biol. 365*, 1176–1186.